Atmos. Chem. Phys. Discuss., 10, 24135–24169, 2010
www.atmos-chem-phys-discuss.net/10/24135/2010/
doi:10.5194/acpd-10-24135-2010

Atmospheric Chemistry and Physics Discussions

Modelled and measured effects of clouds on UV Aerosol Indices on a local, regional, and global scale

M. Penning de Vries and T. Wagner

Max Planck Institute for Chemistry, Mainz, Germany

Received: 9 July 2010 – Accepted: 6 October 2010 – Published: 18 October 2010

Correspondence to: M. Penning de Vries (marloes.penningdevries@mpic.de)

Published by Copernicus Publications on behalf of the European Geosciences Union.

Abstract

The UV Aerosol Indices (UVAI) form one of very few available tools in satellite remote sensing that provide information on aerosol absorption. The UVAI are also quite insensitive to surface type and are determined in the presence of clouds – situations where most aerosol retrieval algorithms do not work. The UVAI are most sensitive to elevated layers of absorbing aerosols, such as mineral dust and smoke from biomass burning, but they can also be used to study non-absorbing aerosols, such as sulphate and secondary organic aerosols. Although UVAI are determined for cloud-contaminated pixels, clouds do affect the value of UVAI in several ways. One way to correct for these effects is to remove clouded pixels using a cloud filter. However, this causes a large loss of data, biases the results towards clear skies, and removes all potentially very interesting pixels where aerosols and clouds co-exist. We here propose to correct the effects of clouds on UVAI in a more sophisticated way, namely by simulating the contribution of clouds to UVAI, and then subtracting it from the measured data.

To this aim, we modelled UVAI from clouds by using measured cloud optical parameters – either with low spatial resolution from SCIAMACHY, or high resolution from MERIS – as input. The modelled UVAI were compared with UVAI measured by SCIAMACHY on different spatial (local, regional and global) and temporal scales (single measurement, daily means and seasonal means). The general dependencies of UVAI on cloud parameters were quite well reproduced, but several issues remain unclear: compared to the modelled UVAI, measured UVAI show a bias, in particular for large cloud fractions, and much larger scatter. Also, the viewing angle dependence differs for measured and modelled UVAI.

The modelled UVAI from clouds will be used to correct measured UVAI for the effect of clouds, thus allowing a more quantitative analysis of UVAI and enabling investigations of aerosol-cloud interactions.

ACPD

10, 24135–24169, 2010

1 Introduction

Aerosol particles are an important constituent of the atmosphere, as they perturb the distribution of solar radiation directly (by scattering and absorbing radiation) and indirectly (by affecting cloud properties), and influence atmospheric chemistry in a passive (as a catalyst or by providing a reaction surface) and active sense (e.g., Seinfeld and Pandis, 1998; Pöschl, 2005). The effects of an aerosol layer on its surroundings – properties of clouds, boundary layer and surface temperature (Andreae and Rosenfeld, 2008; Koren et al., 2008; Rosenfeld et al., 2008; Davidi et al., 2009) – and hence on climate depend strongly on the absorptive properties of the aerosol particles. Despite the importance of information on aerosol absorption for accurate assessment of aerosol radiative effects, however, it is not well quantified on a global scale. The reason is that aerosol optical properties are difficult to determine by remote sensing.

The UV Aerosol Indices (UVAI), which are a measure of spectral contrast in the UV range, form a useful tool to study aerosol absorption: they are highly sensitive to aerosols that absorb UV radiation, they are relatively insensitive to surface type, and they are determined for cloudy as well as clear scenes. In the past, UVAI have mostly been applied to the study of UV-absorbing aerosols, such as mineral dust and smoke (e.g., Hsu et al., 1996, 2003; Herman et al., 1997; Gleason et al., 1998; Chiapello et al., 1999; Mahowald and Dufresne, 2004; Darmenova et al., 2005; Fromm et al., 2006; de Graaf et al., 2007). We have recently shown that aerosols that barely absorb UV radiation, here termed "scattering aerosols", can also be studied using UVAI, if its negative scale is regarded (Penning de Vries et al., 2009). If aerosol radiative effects are to be quantified on a global scale, both scattering and absorbing aerosols have to be taken into account, thus it is necessary to study the whole scale of UVAI.

The quantitative interpretation of UVAI is not straightforward due to the strong dependence of UVAI on aerosol properties, in particular the layer altitude (ALH), aerosol optical thickness (AOT), and single-scattering albedo (SSA). One way to disentangle these influences is to take AOT and ALH from other satellite observations, as was re-

ACPD
10, 24135–24169, 2010

cently shown in a paper by Jeong and Hsu, who presented a method to derive SSA of smoke particles by the combination of CALIOP ALH, MODIS AOT and OMI UV Aerosol Index (Jeong and Hsu, 2008). Similar studies exploiting the strengths of different satellite instruments were presented recently, combining TOMS and MODIS (Hu et al., 2007), OMI and CALIOP (Dirksen et al., 2009; Guan et al., 2010), or MODIS and OMI (Satheesh et al., 2009).

Another complicating issue in the way of quantitative application of the UVAI are the effects of clouds, particularly for satellite instruments with large footprints (e.g., SCIAMACHY, GOME-2, OMI), where completely cloud-free scenes are rare (Krijger et al., 2007). Clouds have various effects on UVAI: (1) when aerosols are present, clouds may shield a lower-lying aerosol layer from view. Alternatively (2), when clouds are located below the aerosol layer they may enhance the apparent surface albedo, significantly increasing the sensitivity of UVAI to aerosol absorption (Torres et al., 1998; Hsu et al., 1999, 2003; de Graaf et al., 2005). Much less known is the fact (2) that clouds also have an own contribution to UVAI (Penning de Vries et al., 2009). This contribution can be quite substantial for broken clouds: up to −1.5 units in magnitude. Because the cloud contribution to UVAI is negative, including cloud-contaminated pixels in temporal or spatial averages may lead to average UVAI values that are systematically too small.

The effects of clouds can be reduced by applying a cloud filter, but this means that a lot of (potentially very interesting) data are discarded. This also causes datasets to be biased to cloud-free scenes, and makes it impossible to study aerosol-cloud interactions. Another way to deal with clouds is to model their contribution to UVAI and subtract it from the measured UVAI. For our cloud correction method to succeed, the dependence of UVAI from clouds (cloudUVAI) on cloud parameters and measurement geometry needs to be known quite accurately. Here, we only address the own contribution of clouds to UVAI (2), thereby solely accounting for one of the effects of clouds on UVAI. The study of the other two effects of clouds (1 and 2) mentioned above is the subject of a forthcoming publication, but will be included in a future, more complete cloud correction scheme.

ACPD
10, 24135–24169, 2010

In this paper, we show that the contribution of clouds to UVAI can be well modelled if the cloud fraction is known, and even better if some information on cloud heterogeneity is available. We first present a comparative case study where cloudUVAI was determined once using low-resolution SCIAMACHY cloud fractions, and once using collocated, high-resolution MERIS cloud optical thickness. Next, we show a study of the dependence of measured and modelled SCIAMACHY UVAI on cloud fraction for a remote ocean region. Finally, we present a global view of cloudUVAI, and demonstrate the effect of cloud filtering on seasonally averaged UVAI.

2 Method

2.1 UV Aerosol Indices

The UVAI are a measure of the spectral contrast of a scene relative to the spectral contrast for a modelled scene where only Rayleigh scattering takes place (Herman et al., 1997; Torres et al., 1998). Its sensitivity to aerosols arises from the fact that an aerosol layer shields the underlying atmosphere, so that less Rayleigh scatter events take place. Since the wavelength dependence of aerosol optical parameters differs from that of molecules, the aerosol layer causes a change in contrast between a wavelength λ and a reference wavelength λ_0 in the UV range. The UVAI are calculated by modelling an atmosphere devoid of aerosols bounded by a Lambertian reflector with a certain albedo value. The albedo is chosen so that the modelled reflectance at λ_0 matches the measured reflectance at λ_0. The ratio between the measured and modelled reflectance at λ then gives the UVAI (Torres et al., 1998):

$$\mathrm{UVAI} = -100 \cdot^{10} \log \left(\frac{R^{\mathrm{meas}}}{R^{\mathrm{Rayl}}} \right)_{\lambda} \quad (1)$$

with R^{meas} and R^{Rayl} the measured and modelled reflectances at wavelength λ, respectively.

ACPD
10, 24135–24169, 2010

The positive part of UVAI is commonly defined as the Absorbing Aerosol Index (AAI); whereas the negative part is defined as the SCattering Index, or SCI (Penning de Vries et al., 2009):

AAI=UVAI for UVAI≥0, undefined for UVAI<0 (2a)

SCI=UVAI for UVAI≤0, undefined for UVAI>0 (2b)

Our UVAI algorithm for SCIAMACHY was described in detail in Penning de Vries et al. (2009), but will be explained shortly here. For each SCIAMACHY pixel, UVAI are determined from the measured reflectances at λ=335.5 nm and λ_0=376.5 nm by using a look-up-table (LUT). The LUT contains reflectances at λ and λ_0 for all combinations of solar zenith angle (SZA) between 15° and 80°, line-of-sight zenith angle (LZA) from 0° to 35°, relative azimuth angle (RAZI) from 0° to 180°, and surface height from 0 to 7 km, computed using the vector version of the SCIATRAN3.0 radiative transfer model (Rozanov et al., 2002, 2005). The LUT is interpolated to yield R^{Rayl}, which is then inserted into Eq. (1) to give the UVAI.

We have estimated the error for our results from SCIAMACHY to be on the order of 0.2–0.3 UVAI units. Larger (systematic) errors may arise over surfaces with strong spectral dependence in the UV range (desert, "coloured" ocean regions, see also Sect. 4.3), or due to strong altitude gradients within a satellite ground pixel. These issues are discussed in more detail in Penning de Vries et al. (2009).

2.2 Satellite instruments

The SCanning Imaging Absorption spectroMeter for Atmospheric CHartographY (SCIAMACHY) and the MEdium Resolution Imaging Spectrometer (MERIS) are two of ten instruments that make up the payload of ESA's ENVISAT satellite. ENVISAT was launched in March, 2002, into a descending polar orbit located at approximately 800 km from the Earth's surface. It passes the equator at a local time of 10:00 a.m.

SCIAMACHY was developed to measure the gaseous composition of the Earth's atmosphere (Bovensmann et al., 1999; Wagner et al., 2008) by use of Differential

ACPD
10, 24135–24169, 2010

Optical Absorption Spectroscopy (DOAS, Platt and Stutz, 2008). The instrument has a moderate spectral resolution, typically 0.2–0.4 nm, but quite poor spatial resolution: generally, the ground pixel size is 30×60 km^2. SCIAMACHY's swath is 1000 km wide, and global coverage is achieved approximately every 6 days. The feature that makes SCIAMACHY unique is the limb-nadir matching procedure, which allows collocated measurements of the total column of a trace gas (in nadir geometry) and its stratospheric profile (in limb geometry). The limb-nadir matching is the reason for the division of the orbit into blocks of (generally) 260 measurements, called states.

The MERIS instrument was primarily developed to measure ocean colour (phytoplankton, coloured dissolved organic matter and suspended matter) over coasts and open ocean, clouds and water vapour concentrations in the atmosphere, and vegetation patterns over land (Bézy et al., 2000). MERIS detects Earth's reflectance in 15 programmable bands between 390 nm and 1040 nm with a spatial resolution of 1.04×1.2 km^2 over ocean. MERIS' swath is 1150 km wide, and global coverage is achieved every three days. For our investigations, we used the MERIS operational level-2 cloud optical thickness product, which was obtained from (http://merci-srv.eo.esa.int/merci/queryProducts.do).

2.3 Radiative transfer modelling

The radiative transfer modelling performed for this paper was done using the vector version discrete ordinate method (in plane-parallel atmosphere) implemented in SCIATRAN3.0 (downloaded from: http://www.iup.physik.uni-bremen.de/sciatran/downloads/), which is the successor to SCIATRAN2.0 (Rozanov et al., 2002, 2005).

For the modelling of clouds, we used the Henyey-Greenstein parameterisation (Henyey and Greenstein, 1941): clouds were assumed to be non-absorbing in the visible wavelength range (SSA=1.00), the asymmetry parameter g was set to 0.87, a value considered appropriate for water clouds (Wendisch et al., 2005), except in one case in Sect. 3.1, where g was set to 0.75 (representative for ice clouds) in a sensitivity test. Cloud optical thickness was assumed to be spectrally independent.

ACPD
10, 24135–24169, 2010

3 Theory

3.1 Cloud dependence of UV Aerosol Indices

Clouds are complex three-dimensional structures that can be very inhomogeneous in their horizontal and vertical extent. Passive remote sensing satellite instruments such as SCIAMACHY and MERIS cannot resolve sub-pixel cloud structures, therefore their cloud detection algorithms typically retrieve averaged (or effective) cloud properties. Such algorithms make use of the change in reflectance at the top of the atmosphere caused by the presence of clouds. The reflectance in the visible range is mostly determined by the fraction of the pixel covered by the cloud (geometrical cloud fraction, CF_{geom}), and the cloud top albedo, which depends on cloud optical thickness (COT) in a non-linear fashion. If a satellite pixel is completely covered by clouds and if the clouds are assumed to be homogeneous throughout the satellite pixel, COT can be determined directly from the top-of-atmosphere reflectance. Due to the coarse spatial resolution of SCIAMACHY most pixels are only partially covered by clouds and usually only an effective cloud fraction (CF_{eff}) is determined. The CF_{eff} is a linear function of CF_{geom} and cloud albedo, and is quite well suited to account for the effects of clouds on trace gas retrievals (Wang et al., 2008). The definition of CF_{eff} in this paper is analogous to the definition of CF_{eff} in the FRESCO+ (Koelemeijer et al., 2001; Wang et al., 2008) and HICRU (Grzegorski et al., 2006) cloud retrieval algorithms:

$$CF_{eff} = \left(\frac{R^{meas} - R^{clear}}{R^{cloudy} - R^{clear}} \right)_{\lambda=758} \quad (3)$$

where R^{meas} is the measured reflectance at 758 nm, R^{clear} the reflectance under cloud- and aerosol-free conditions, and R^{cloud} the reflectance of a pixel completely covered by a homogeneous cloud with an albedo equal to 0.80 (equivalent to a COT of 50). A major shortcoming of CF_{eff} is the fact that it cannot discriminate between homogeneous and heterogeneous (or: optically thin and optically thick) clouds: for example, a CF_{eff}

ACPD
10, 24135–24169, 2010

of 0.5 can be due to clouds with a cloud albedo of 0.8 (COT = 50) covering 50% of the pixel, by clouds with a cloud albedo of 0.4 (COT = 10) covering the complete pixel, or anything in between.

The dependence of cloudUVAI (the contribution of a cloud to the UVAI) on CF_{eff} is determined by the sub-pixel structure of the cloud. In this paper, we assume that the cloud is sufficiently described by COT and CF_{geom} – an assumption that is shown to be valid for our purposes in Sect. 4.1. Because those two quantities cannot be disentangled using the FRESCO+ or HICRU algorithms, we study two extreme cases: "thick clouds", which are clouds with COT=50, but varying CF_{geom}, of which the reflectances were calculated using the independent pixel approximation. And "thin clouds", which are homogeneous clouds with CF_{geom}=1 and varying COT. In Penning de Vries et al. (2009) the modelled dependence of UVAI on CF_{eff} was shown for thick and for thin clouds, and it was found that the UVAI does not depend strongly on cloud altitude. The results from a similar model study are shown in Fig. 1, where the panels on the left and right of the figure show results for thick and thin clouds, respectively. These were obtained by modelling the clouds using the Henyey-Greenstein parameterization (HG clouds), as described in Sect. 2.3. The results are shown for nadir viewing geometry and three different SZAs of 20°, 40° and 60°, in blue, green, and red, respectively. For the results connected by solid lines, the cloud parameters were the same as in Penning de Vries et al. (2009), and representative of a water cloud: single-scattering albedo was equal to 1.00, and the asymmetry parameter g was set to 0.87 (Wendisch et al., 2005). The dotted lines connect the results calculated with g=0.75, which is probably more representative of ice clouds (Wendisch et al., 2005). Clouds were assumed to be homogeneous layers with a geometrical thickness of 1 km, starting at the surface. UVAI is plotted against CF_{eff}, which is equal to CF_{geom} for the thick clouds in the left panel in Fig. 1, and is determined from the modelled reflectance at 758 nm according to Eq. (3) for the right panel (thin clouds). By definition, UVAI at CF_{eff}=0 and CF_{eff}=1, respectively, are identical for thick and thin clouds.

ACPD
10, 24135–24169, 2010

As seen in Fig. 1, when CF_{eff} is higher than approximately 0.7 the cloud type (thick or thin) is not of great importance to UVAI: cloudUVAI is very similar in both panels for clouds with large CF_{eff} when SZA<60°. For smaller CF_{eff}, however, there can be a difference of up to one UVAI unit (in particular for large SZA) between the two different cloud models shown in Fig. 1. It can also be seen that the asymmetry parameter has some influence on UVAI, especially for thick clouds, but the effect is not very large – on the order of 0.1–0.2 UVAI units.

Figure 2 displays the results obtained when the cloud is modelled as a Lambertian surface with albedo equal to 0.80. The cloud described by the Lambertian reflector (Lambertian cloud) is modelled using the independent pixel approximation, in analogy to the thick HG cloud. To improve the comparison with Fig. 1, the Lambertian cloud was set to an altitude of 1 km, although this changed the UVAI values by less than 0.05 units with respect to a Lambertian reflector at 0 km altitude. It is interesting to note here that a pixel with highly heterogeneous surface albedo in the UV range, e.g., an ocean pixel partially covered by ice, will yield a UVAI value very similar to an ocean pixel partially covered by a Lambertian cloud.

The differences between the two thick cloud models – the HG cloud and the Lambertian cloud – are worth discussing in more detail. For small SZA, the differences are rather small, although for the HG cloud, cloudUVAI deviates appreciably from 0 for CF_{eff}=1, which is not seen for the Lambertian cloud. As SZA increases, the deviation between the HG cloud and the Lambertian cloud increases; even the direction of the change in cloudUVAI with increasing SZA is different: for the Lambertian cloud, cloudUVAI decreases slightly with SZA, whereas for the HG cloud, cloudUVAI increases. The reason for these differences is most probably the angular dependence of the light scattered by the model cloud. Whereas scattering by the Lambertian cloud is isotropic by definition, the HG cloud scatters mostly in the forward direction by the choice of g=0.87 (or even 0.75). This is what causes the differences in dependence on SZA and viewing geometry (not shown here). Although the Henyey-Greenstein parameterisation of clouds is better than the assumption of a Lambertian reflector, it is still not completely

ACPD
10, 24135–24169, 2010

accurate: the choice of an asymmetry parameter instead of a full scattering phase function affects the amount of modelled backscattering. This, in turn, influences the modelled dependence of cloudUVAI on solar and viewing angles.

We extended the model study to investigate the dependence of cloudUVAI on cloud top height and on the instrument viewing angle in more detail. The results are shown in Fig. 3 for thick clouds (dots, solid lines) and thin clouds (triangles, dashed lines) for three values of SZA. The left panel of Fig. 3 confirms the finding in Penning de Vries et al. (2009), that cloudUVAI does not depend strongly on cloud top height. In the figure we only show the results for a medium-sized cloud (CF_{eff}=0.4), but other simulated clouds show the same behaviour.

The viewing angle dependence of UVAI is, on the other hand, quite significant. This is illustrated in the right panel of Fig. 3 for the medium-sized cloud (CF_{eff}=0.4) with a cloud top height of 1 km. The viewing angle dependence is most pronounced for thin clouds, and increases with increasing SZA. The most drastic effects are seen for the positive viewing angles, representing the eastern part of SCIAMACHY's swath, and imply an intrinsic east-west bias of cloudUVAI for cases where SZA is larger than about 20°. The scatter on the curves in the right panel of Fig. 3 is caused by small errors in the calculated cloud reflectances.

3.2 Calculation of cloudUVAI from satellite data

We have calculated cloudUVAI from HICRU effective cloud fractions and cloud top height for the whole SCIAMACHY dataset. For this, we used two separate look-up-tables (LUTs): one for thick clouds with geometrical cloud fractions between 0 and 1 (and COT = 50), and the other for thin clouds with cloud optical thickness between 0 and 50 (and CF_{geom}=1). The LUTs of cloudUVAI contain all combinations of viewing angles and solar zenith angles relevant for this study (SZA 15°–60°, LZA 0°–35°, RAZI 0°–180°). The weak dependence of cloudUVAI on cloud altitude is taken into account by including clouds with cloud top heights ranging from 1 to 15 km.

ACPD
10, 24135–24169, 2010

In Figs. 5 and 6, we present the results from a case study where modelled cloudUVAI, both for the thick cloud and thin cloud assumption, are compared to UVAI measured by SCIAMACHY. We also include a comparison to cloudUVAI calculated from spatially higher resolved MERIS cloud optical thickness. The different ways of calculating cloudUVAI from cloud parameters from either SCIAMACHY (HICRU) or MERIS are illustrated schematically in Fig. 4. In the figure, ovals denote high spatial resolution ($1\times1\,km^2$, MERIS resolution), whereas rectangles indicate SCIAMACHY resolution ($30\times60\,km^2$). For SCIAMACHY, the calculation of UVAI and cloudUVAI are quite straightforward, and were described above (in Sects. 3.1 and 3.2, respectively). For the MERIS data, different approaches were tested. The simplest way is to regrid the high-resolution cloud data to SCIAMACHY resolution (arrow 1 in Fig. 4), then calculating cloudUVAI from it (arrow 2 and box marked "Z"). A more accurate way is to do the calculation of MERIS cloudUVAI in two steps: first, from a LUT similar to the ones described above, reflectances at the UVAI wavelengths of 335.5 and 376.5 nm were determined from MERIS COT (arrow 3), assuming that clouds homogeneously cover MERIS pixels with non-zero COT (thin cloud assumption). Subsequently, these reflectances were converted to UVAI values by passing them to our standard UVAI algorithm (described in Sect. 3; arrow 6 in Fig. 4). We also gridded the obtained MERIS-resolution cloud reflectances to the much coarser SCIAMACHY resolution (arrow 4), and subsequently converted these reflectances to UVAI (arrow 5). The reason for this two-step approach is that the boxes marked "G" and "X" in Fig. 4 are not equivalent: since UVAI depend non-linearly on the input reflectances, UVAI cannot simply be averaged over two (or more) MERIS pixels. Instead, the (modelled) UV reflectances need to be averaged, and the UVAI should be determined from the resulting reflectances. It was verified that the direct approach (where cloudUVAI is directly read from the LUT) and indirect approach (via cloud reflectances) are equivalent by comparing the data marked "F" in Fig. 4 with cloudUVAI determined directly from MERIS COT (not shown).

ACPD
10, 24135–24169, 2010

4 Results

4.1 Case studies: cloudUVAI from MERIS and SCIAMACHY cloud parameters

For our case studies we selected two scenes from orbit 191 033 of ENVISAT, performed on 16 January 2005. Both are located over the Pacific Ocean, where aerosol concentrations are expected to be small. This was verified by comparison with MODIS AOT, which did not exceed 0.1 for the unclouded pixels (MODIS AOT downloaded from the LAADS website: http://ladsweb.nascom.nasa.gov/index.html). According to our model calculations, a low-lying, non-absorbing aerosol layer (e.g., sea-spray aerosols) with an AOT of 0.1 does not significantly affect UVAI (not shown).

Figure 5 displays the cloud field as measured by MERIS (COT, panel A) and by SCIAMACHY (CF_{eff}, panel B) for SCIAMACHY states 8 and 9 (M-Factor enumeration). The selected scene contains a high, narrow cloud with high COT in the Northwest, some small scattered clouds in the East of the swath, and a largely clear scene in the Southeast. Panel C shows the SCIAMACHY UVAI, which displays enhanced SCI values for the clouded pixels: the cloud structures can be clearly recognized in the UVAI plot. In panels D and E, cloudUVAI determined from HICRU CF_{eff} are shown for the thick and thin cloud assumption, respectively. Whereas the cloud structures are still vaguely recognizable in panel D (thick cloud assumption), the pattern in panel E (thin cloud assumption) is quite different, emphasizing the (modelled) difference in radiative properties between heterogeneous and completely homogeneous clouds. In panel F and G, cloudUVAI calculated from MERIS COT are shown at MERIS and at SCIAMACHY resolution, respectively. For panel G, the cloud reflectances calculated from MERIS COT were averaged to SCIAMACHY resolution, after which the UVAI were determined (see Sect. 3.2 and Fig. 4), which explains the slight differences between panels F and G. The viewing angle dependence of cloudUVAI (see Sect. 3.1) is most pronounced in panel F. The spatial agreement between measured UVAI and cloudUVAI from MERIS COT is good, as seen upon comparison of panels C and G. The value of UVAI, however, is much smaller (SCI is larger) for the data measured by SCIAMACHY

ACPD
10, 24135–24169, 2010

than for any of the calculated cloudUVAI values. The reason for this discrepancy is not clear, but we speculate that remaining errors in SCIAMACHY's calibration may be the cause. Another possibility is that the clouds are not modelled accurately enough. These issues will be discussed further in Sect. 5.

The cloud field in states 15 and 16 of the same orbit as shown in Fig. 5 was quite different (Fig. 6, panels A and B): a large part of the pixels was covered by a thick, low cloud. SCIAMACHY detected quite low UVAI (high SCI) for most of the scene, as shown in panel C. Pixels flagged as having "sun-glint risk" were discarded from both the SCIAMACHY and MERIS datasets.

Again, the spatial patterns of cloudUVAI calculated from HICRU parameters using the thick cloud assumption are more in agreements with the measured UVAI than the cloudUVAI calculated using the thin cloud assumption, as seen when comparing panel C with panels D and E. Using MERIS COT as input for the cloudUVAI calculations slightly improves the spatial correspondence, although, as noted for states 8 and 9, the measured UVAI values are too small in comparison to the modelled values.

In both of the case studies presented above, the best agreement between measured UVAI and modelled cloudUVAI was found when cloudUVAI were calculated from high-resolution MERIS COT. Unfortunately, it would be computationally too expensive to apply this method to the whole SCIAMACHY dataset. For this reason, we also determined cloudUVAI using SCIAMACHY-resolution cloud parameters recalculated from MERIS COT (arrows 1 and 2 and box marked "Z" in Fig. 4). The results were very similar to those displayed in panels G of Figs. 5 and 6, and are therefore not shown here. This finding implies that the exact structure of the cloud is not of much importance to the cloudUVAI and that the description of clouds by COT and CF_{geom} is sufficient for our purpose.

4.2 Dependence of cloudUVAI on CF_{eff}

We have studied daily averaged values of UVAI from SCIAMACHY and cloudUVAI calculated from HICRU cloud parameters over remote ocean regions, where the

ACPD
10, 24135–24169, 2010

concentration of aerosols is assumed to be small. The region is also not significantly affected by ocean colour. The results were binned by SZA, viewing geometry, and CF_{eff}, and subsequently averaged by day or by season. Pixels in sun glint geometry were discarded.

Figure 7 shows the average UVAI obtained for the period January–March 2005, for the region located between 20–40° S and 100–180° W. Only pixels in near-nadir geometry (LZA between −10° and +10°) are plotted, divided into three different SZA bins: 30°–40° (upper left panel), 40°–50° (upper right panel), and 50°–60° (lower panel). Measured UVAI data are shown in blue with dots representing daily averages and the size of the dot indicating the number of observations; lines connect the seasonal averages. The cloudUVAI calculated with the thick cloud assumption are depicted in green, and cloudUVAI calculated with the thin cloud assumption in red. Error bars on the modelled cloudUVAI indicate the spread of the data (i.e., the maximum and minimum daily averaged cloudUVAI).

In Fig. 7, it can be seen that the dependence of the seasonally averaged measured UVAI (blue) is in good agreement with the modelled cloudUVAI dependence (compare Fig. 1). The shape of the measured UVAI dependence on CF_{eff} is quite well described by the model calculations, although there is a disagreement for $CF_{eff}>0.8$, and the variability in daily averaged UVAI is also not well reproduced (indicated by the error bars on the green and red cloudUVAI lines). An examination of the results for other viewing geometries, which are not shown here, revealed that the dependence of measured UVAI on viewing angle was not well reproduced by the modelled cloudUVAI (see Fig. 3). It is not clear what the reason for these discrepancies is, although we suspect calibration errors of SCIAMACHY to be a factor, as well as the inaccurate description of clouds in our radiative transfer model calculations. This will be discussed in further detail in Sect. 5.

ACPD
10, 24135–24169, 2010

4.3 Global maps of cloudUVAI

In Figs. 8–10, we present UVAI results for seasonal averages over the months January–March 2005, sorted by HICRU effective cloud fraction: the left column of Fig. 8 contains only scenes with CF_{eff}<5%; the right column has CF_{eff} between 5% and 25%; the left and right columns of Fig. 9 contain scenes with CF_{eff} 25–50% and CF_{eff} 50%–100%, respectively; and Fig. 10 shows the unfiltered seasonal averages. The rows contain (from top to bottom): SCIAMACHY average UVAI (A), cloudUVAI calculated from HICRU CF_{eff} for thick clouds (B) and thin clouds (C), difference between UVAI and cloudUVAI for thick clouds (D) and thin clouds (E), and average HICRU CF_{eff} (F). Pixels at the extreme east of SCIAMACHY's swath have been removed, as were pixels in sun-glint geometry, and pixels influenced by snow or ice (regardless of effective cloud fraction).

The most prominent UVAI signals seen in panels A of Figs. 8–10 are observed over the continents, and are almost exclusively UV-absorbing aerosols, such as mineral dust (observed over the Sahara, the Arabian Peninsula, and the Taklimakan Desert) and smoke from burning biomass (over the Sahel region and Southeast Asia). Scattering aerosols are observed in Figs. 8 and 10 over Central Africa, as indicated by negative UVAI (positive SCI). When comparing panels A1 and A2 in Fig. 8, the effect of cloud-screening is immediately recognized: most of the oceans have SCI of approximately 1 in A2 (where CF_{eff} is between 5% and 25%), whereas in A1, UVAI in most ocean regions is near zero. The extended ocean patches in panel A1 where SCI remains between 0.5 and 1 are recognized as regions with enhanced chlorophyll absorption by comparing with monthly averaged MODIS ocean colour maps (obtained from: http://oceancolor.gsfc.nasa.gov/). The bright red spot in Venezuela is located at the Guiana Highlands, is most probably an artefact of the UVAI algorithm's sensitivity to altitude gradients (see Penning de Vries et al., 2009), and may be ignored.

As expected, the effect of clouds in panel A1 is small and rather homogeneous, as seen in the small SCI calculated for thick and thin clouds, shown in panels B1

ACPD
10, 24135–24169, 2010

and C1, respectively. Removing the cloud effects, by subtracting the cloudUVAI from the measured UVAI, therefore does not have a large effect on the global pattern of UVAI (panels D1 and E1). Nevertheless, it can be seen that the thin cloud assumption slightly overestimates the effect of clouds in comparison to the thick cloud assumption: the Southern Hemisphere appears bluer in panel E1 than in panel D1. This may be an indication that small values of CF_{eff} are most frequently caused by clouds with small CF_{geom}, rather than clouds with small cloud top albedo. In panel F1, the average CF_{eff} is shown.

Panels A, D, and E in the right column of Fig. 8 show similar aerosol patterns as those on the left of the figure. Some differences can be observed, in particular in the Sahel biomass burning region, where UVAI has increased, indicating that absorbing aerosols are present in pixels contaminated by significant amounts of clouds. Also, the large plume of absorbing aerosols that is transported south-westward from Northern Africa to South America is more clearly seen in panels A2, D2, and E2. These might be aerosols over or near clouds, but it may also be the result of HICRU's misclassification of mineral dust plumes as clouds. Again, the thin cloud assumption appears to be overestimating the cloud effect in comparison to the thick cloud assumption (compare panels D2 and E2).

Panels A4 and A3 in Fig. 9 are clearly dominated by the cloud signal, as can be seen by comparison with the respective panels B and C. Yet, a significant positive UVAI is observed over the biomass-burning regions: smoke from the Sahel region is seen in panels A3, D3, and E3, whereas the smoke from agricultural fires in Southeast Asia is prominent in the corresponding panels on the right (A4, D4, and E4). Smoke aerosols in Southeast Asia appear to be generally associated with effective cloud fractions larger than 50%. Applying a cloud filter such as the one used to obtain panel A1 of Fig. 8 thus causes the loss of nearly all pixels with smoke aerosols in this region. This needs to be kept in mind when instruments with large footprints, such as SCIAMACHY, are used for aerosol or trace gas retrieval.

ACPD
10, 24135–24169, 2010

Panels D3, D4, E3 and E4 in Fig. 9 show that, in contrast to the results shown in Fig. 8, cloudUVAI determined using the thin cloud assumption are in better agreement with the measured UVAI than cloudUVAI from the thick cloud assumption, which overestimate the cloud effect over most of the globe. In fact, cloudUVAI determined using the thin cloud assumption are slightly too small (in an absolute sense) compared to the measured UVAI: panel E4 is mostly yellowish instead of the expected grey colour of near-zero UVAI. This implies that "true" clouds are neither thick nor thin, but something in between (i.e., COT<50 and CF_{geom}<1). But it may also be a further indication of our inability to correctly model clouds using Henyey-Greenstein parameterisation – an issue that we also mentioned in Sects. 4.1 and 4.2 that might explain (at least some of) the discrepancies between measured and modelled UVAI seen in Figs. 5–7.

The data shown in Fig. 10 have not been cloud-filtered. The figure shows the strength of our method of cloud correction: by subtracting cloudUVAI instead of filtering out the cloud-contaminated pixels, many features seen in panels D1 and E1 in Fig. 8 can be seen in panels D5 and E5 in Fig. 10, including the effects of ocean colour. Yet, all signals from aerosols in cloudy pixels that are missing in Fig. 8, most prominently the biomass burning smoke in Southeast Asia, are retained in Fig. 10. Again, as mentioned above, clouds appear to be neither purely "thick" nor "thin": the thick cloud assumption gives cloudUVAI that are too small (SCI too large) for the oceans south of about 40° S, whereas the thin cloud assumption underestimates the cloud effects there, yielding too large cloudUVAI (SCI too small).

5 Discussion

By comparing measurements and model outcomes on different geographical scales (from local to regional and global) and time scales (from single measurements to daily and seasonal averages), we have shown that clouds cause significant UVAI. As already noted in an earlier study (Penning de Vries et al., 2009), cloud-caused UVAI (here termed "cloudUVAI") can be quite substantial and should be taken into

ACPD
10, 24135–24169, 2010

account, especially if spatial or time averages are being made. An accurate correction of the effect of clouds on UVAI is an important step towards the detection and quantitative analysis of aerosols in the presence of clouds. It was also shown here that applying a cloud filter to satellite measurements with coarse spatial resolution (e.g., SCIAMACHY, GOME-2, OMI) causes the loss of potentially interesting scenes where aerosols are associated with clouds.

From the case studies presented in Sect. 4.1, we found that the spatial resolution of cloud retrieval algorithms based on SCIAMACHY measurements only does not suffice to accurately model the influence of clouds on UVAI. Reasonable agreement was found for cloudUVAI calculated from HICRU effective cloud fractions when clouds were assumed to be optically thick, but the agreement improved considerably when cloudUVAI were calculated from much higher resolved MERIS cloud optical thickness data. Clearly, even the 8-fold increased spatial resolution of HICRU (Grzegorski et al., 2006), which is based on reflectances from SCIAMACHY's PMDs (polarisation measurement devices), does not suffice for the calculation of cloudUVAI. Unfortunately, the large amount of MERIS data makes the calculation of cloudUVAI in this fashion computationally very expensive. A good compromise would be to use MERIS COT to calculate CF_{geom} and average COT for each SCIAMACHY pixel, and calculate cloudUVAI from them (see Fig. 4, box marked "Z"). This approach was found to yield results that were in very good agreement with cloudUVAI calculated from high-resolution MERIS cloud parameters (Sect. 4.1).

In all comparative studies of measured and modelled UVAI presented here, a good qualitative agreement was found, but the values of measured UVAI were generally lower than those modelled. The measured UVAI regularly reached UVAI as small as −2. We have tried to reproduce this value by adjusting the clouds in the model: the asymmetry parameter, g, was varied from 0.87 (representing water clouds) to 0.75, as illustrated in Fig. 1. We also modified the vertical profile of the modelled clouds, varied the albedo of the underlying surface, and tested multiple cloud layers for their effect on cloudUVAI. All changes influenced cloudUVAI on the order of 0–0.4 units,

ACPD
10, 24135–24169, 2010

but in all of these cases cloudUVAI was increased instead of decreased. One possibility remains that the phase function, given by the Henyey-Greenstein asymmetry parameter, may not be accurate enough for cloudUVAI calculation. The application of a double asymmetry parameter (where one describes forward scattering and a second backward scattering) is expected to improve the model results appreciably already, although including a full scattering phase function would be preferable. We are working on an update of the cloudUVAI where an altitude-dependent phase function will be implemented to take into account the different scattering functions of water clouds and ice clouds.

The inaccurate scattering function may also be the reason for the discrepancies between measured UVAI and modelled cloudUVAI shown in Fig. 7: first, the failure of the modelled cloudUVAI to reproduce the measured UVAI dependence on SZA (right panel) or viewing geometry (not shown). And second, the fact that the scatter of the measured daily mean UVAI, which ranges roughly between −2 and +0.5 is larger than that found for the modelled cloudUVAI, which do not go below −1.5 or above 0 (except for large SZA), and generally display a smaller range of values within a single CF_{eff} bin. Another explanation that cannot be ruled out currently is the influence of errors in SCIAMACHY reflectances, in particular those caused by the sensitivity of SCIAMACHY to polarisation, to which UVAI is notoriously sensitive (Tilstra et al., 2007). In the future, we will compare UVAI from other instruments (GOME-2 and OMI) to SCIAMACHY UVAI and modelled cloudUVAI to assess the impact of instrument errors.

6 Conclusions

We have shown that clouds have a significant effect on UV Aerosol Indices (UVAI), and that it is possible to model this effect quite well using simple assumptions on cloud optical parameters. In this paper, we present comparisons between measured and modelled UVAI on a local, regional, and a global scale, and on the levels of a single measurement, daily means and monthly means. Although deficits in the accuracy of

ACPD
10, 24135–24169, 2010

the cloud optical parameters in the model calculations were recognized, the overall agreement between measured and modelled UVAI was good.

The modelled UVAI of a cloud, named "cloudUVAI", can serve to correct for the presence of clouds in UVAI datasets. In contrast to the more generally used cloud filter, subtracting the appropriate cloudUVAI from the data selectively removes the cloud effects without discarding signals from aerosols in (partly) clouded pixels, opening a door to the interesting field of aerosol-cloud interactions.

The presented work addresses only one of three important effects of clouds on aerosols. For an accurate cloud correction of UVAI data, two other effects should also be accounted for: the shielding of lower-lying aerosol layers by clouds and the enhancement of UVAI by clouds underneath aerosol layers due to an apparent increase in surface albedo. We are currently investigating these effects.

Acknowledgement. H. Sihler is acknowledged for critical reading of the manuscript. IUP Bremen, A. Rozanov and V. Rozanov are kindly thanked for providing a pre-release version of SCIATRAN 3.0 (from http://www.iup.physik.uni-bremen.de/sciatran/downloads/), and for their technical support. SCIAMACHY and MERIS data were provided by ESA. The MODIS team and NASA are thanked for making their data freely available via http://ladsweb.nascom.nasa.gov/index.html.

M. P.d.V. acknowledges the Max Planck Society for a research grant.

The service charges for this open access publication
have been covered by the Max Planck Society.

References

Andreae, M. O. and Rosenfeld, D.: Aerosol-cloud-precipitation interactions. Part 1. The nature and sources of cloud-active aerosols, Earth Sci. Rev., 89, 13–41, 2008.

Bovensmann, H., Burrows, J. P., Buchwitz, M., Frerick, J., Noël, S., Rozanov, V. V.,

ACPD

10, 24135–24169, 2010

Chance, K. V., and Goede, A. P. H.: SCIAMACHY: Mission objectives and measurements modes, J. Atmos. Sci., 56, 127–150, 1999.
Chiapello, I., Prospero, J. M., Herman, J. R., and Hsu, N. C.: Detection of mineral dust over the North Atlantic Ocean and Africa with the Nimbus 7 TOMS, J. Geophys. Res., 104(D8), 9277–9291, 1999.
Darmenova, K., Sokolik, I. N., and Darmenov, A.: Characterization of east Asian dust outbreaks in the spring of 2001 using ground-based and satellite data, J. Geophys. Res., 110, D02204, doi:10.1029/2004JD004842, 2005.
Davidi, A., Koren, I., and Remer, L.: Direct measurements of the effect of biomass burning over the Amazon on the atmospheric temperature profile, Atmos. Chem. Phys., 9, 8211–8221, doi:10.5194/acp-9-8211-2009, 2009.
de Graaf, M., Stammes, P., Torres, O., and Koelemeijer, R. B. A.: Absorbing aerosol index – sensitivity analysis, application to GOME and comparison with TOMS, J. Geophys. Res., 110, D01202, doi:10.1029/2004JD005178, 2005.
de Graaf, M., Stammes, P., and Aben, E. A. A.: Analysis of reflectance spectra of UV-absorbing aerosol scenes measured by SCIAMACHY, J. Geophys. Res., 112, D02206, doi:10.1029/2006JD007249, 2007.
Dirksen, R. J., Boersma, K. F., de Laat, J., Stammes, P., van der Werf, G. R., Val Martin, M., and Kelder, H. M.: An aerosol boomerang: rapid around-the-world transport of smoke from the December 2006 Australian forest fires observed from space, J. Geophys. Res., 114, D21201, 2009.
Fromm, M., Tupper, A., Rosenfeld, D., Servanckx, R., and McRae, R.: Violent pyro-convective storm devastates Australia's capital and pollutes the stratosphere, Geophys. Res. Lett., 33, L05815, doi:10.1029/2005GL025161, 2006.
Gleason, J. F., Hsu, N. C., and Torres, O.: Biomass burning smoke measured using backscattered ultraviolet radiation: SCAR-B and Brazilian smoke interannual variability, J. Geophys. Res., 103(D24), 31969–31978, 1998.
Grzegorski, M., Wenig, M., Platt, U., Stammes, P., Fournier, N., and Wagner, T.: The Heidelberg iterative cloud retrieval utilities (HICRU) and its application to GOME data, Atmos. Chem. Phys., 6, 4461–4476, doi:10.5194/acp-6-4461-2006, 2006.
Guan, H., Esswein, R., Lopez, J., Bergstrom, R., Warnock, A., Follette-Cook, M., Fromm, M., and Iraci, L. T.: A multi-decadal history of biomass burning plume heights identified using aerosol index measurements, Atmos. Chem. Phys., 10, 6461–6469, doi:10.5194/acp-10-

ACPD
10, 24135–24169, 2010

6461-2010, 2010.
Henyey, L. and Greenstein, J.: Diffuse radiation in the galaxy, Astrophys. J., 93, 70–83, 1941.
Herman, J. R., Bhartia, P. K., Torres, O., Hsu, C., Seftor, C., and Celarier, E.: Global distribution of UV-absorbing aerosols from Nimbus 7/TOMS data, J. Geophys. Res., 102(D14), 16911–16922, 1997.
Hsu, N. C., Herman, J. R., Bhartia, P. K., Seftor, C. J., Torres, O., Thompson, A. M., Gleason, J. F., Eck, T. F., and Holben, B. N.: Detection of biomass burning smoke from TOMS measurements, Geophys. Res. Lett., 23(7), 745–748, 1996.
Hsu, N. C., Herman, J. R., Gleason, J. F., Torres, O., and Seftor, C. J.: Satellite detection of smoke aerosols over a snow/ice surface by TOMS, Geophys. Res. Lett., 26, 1165–1168, 1999.
Hsu, N., Herman, C. J. R., and Tsay, S.-C.: Radiative impacts from biomass burning in the presence of clouds during boreal spring in southeast Asia, Geophys. Res. Lett., 30, 1224, 2003.
Hu, R.-M., Martin, R. V., and Fairlie, T. D.: Global retrieval of columnar aerosol single scattering albedo from space-based observations, J. Geophys. Res., 112, D02204, doi:10.1029/2005JD006832, 2007.
Jeong, M.-J. and Hsu, N. C.: Retrievals of aerosol single-scattering albedo and effective aerosol layer height for biomass-burning smoke: synergy derived from “A-Train” sensors, Geophys. Res. Lett., 35, L24801, doi:10.1029/2008GL036279, 2008.
Koelemeijer, R. B. A., Stammes, P., Hovenier, J. W., and de Haan, J. F.: A fast method for retrieval of cloud parameters using oxygen A band measurements from the Global Ozone Monitoring Experiment, J. Geophys. Res., 106, 3475–3490, 2001.
Koren, I., Vanderlei Martins, J., Remer, L. A., and Afargan, H.: Smoke invigoration versus inhibition of clouds over the Amazon, Science, 321, 946–949, 2008.
Krijger, J. M., van Weele, M., Aben, I., and Frey, R.: Technical Note: The effect of sensor resolution on the number of cloud-free observations from space, Atmos. Chem. Phys., 7, 2881–2891, doi:10.5194/acp-7-2881-2007, 2007.
Mahowald, N. M. and Dufresne, J.-L.: Sensitivity of TOMS aerosol index to boundary layer height: implications for detection of mineral aerosol sources, Geophys. Res. Lett., 31, L03103, doi:10.1029/2003GL018865, 2004.
Penning de Vries, M. J. M., Beirle, S., and Wagner, T.: UV Aerosol Indices from SCIAMACHY: introducing the SCattering Index (SCI), Atmos. Chem. Phys., 9, 9555–9567,

ACPD
10, 24135–24169, 2010

doi:10.5194/acp-9-9555-2009, 2009.
Platt, U. and Stutz, J.: Differential optical absorption spectroscopy: principles and applications, in: Physics of Earth and Space Environment Series, edited by: Guzzi, R., Lanzerotti, L., and Platt, U., Springer, 2008.
Pöschl, U.: Atmospheric aerosols: composition, transformation, climate and health effects, Angew. Chem. Int. Ed., 44, 7520–7540, 2005.
Rosenfeld, D., Lohmann, U., Raga, G. B., O'Dowd, C. D., Kulmala, M., Fuzzi, S., Reissell, A., and Andreae, M. O.: Flood or drought: how do aerosols affect precipitation, Science, 321, 1309–1313, 2008.
Rozanov, V. V., Buchwitz, M., Eichmann, K.-U., de Beek, R., and Burrows, J. P.: SCIATRAN – a new radiative transfer model for geophysical applications in the 240–2400 nm spectral region: the pseudo-spherical version, Adv. Space Res., 29(11), 1831–1835, 2002.
Rozanov, A., Rozanov, V., Buchwitz, M., Kokhanovsky, A., and Burrows, J. P.: SCIATRAN 2.0 – a new radiative transfer model for geophysical applications in the 175–2400 nm spectral region, Adv. Space Res., 36, 1015–1019, 2005.
Satheesh, S. K., Torres, O., Remer, L. A., Suresh Babu, S., Vinoj, V., Eck, T. F., Kleidman, R. G., and Holben, B. N.: Improved assessment of aerosol absorption using OMI-MODIS joint retrieval, J. Geophys. Res., 114, D05209, doi:10.1029/2008JD011024, 2009.
Seinfeld, J. H. and Pandis, S. N.: Atmospheric Chemistry and Physics: From Air Pollution to Climate Change, 2nd edn., Wiley, New York, USA, 2006.
Tilstra, L. G., de Graaf, M., Noël, S., Aben, I., and Stammes, P.: SCIAMACHY's absorbing aerosol index and the consequences of instrument degradation, Proc. ACVE-3, 2007.
Torres, O., Bhartia, P. K., Herman, J. R., Ahmad, Z., and Gleason, J.: Derivation of aerosol properties from satellite measurements of backscattered ultraviolet radiation: theoretical basis, J. Geophys. Res., 103(D14), 17099–17110, 1998.
Wagner, T., Beirle, S., Deutschmann, T., Eigemeier, E., Frankenberg, C., Grzegorski, M., Liu, C., Marbach, T., Platt, U., and Penning de Vries, M.: Monitoring of atmospheric trace gases, clouds, aerosols and surface properties from UV/vis/NIR satellite instruments, J. Opt. A: Pure Appl. Opt., 10, 104019, doi:10.1088/1464-4258/10/10/104019, 2008.
Wang, P., Stammes, P., van der A, R., Pinardi, G., and van Roozendael, M.: FRESCO+: an improved O_2 A-band cloud retrieval algorithm for tropospheric trace gas retrievals, Atmos. Chem. Phys., 8, 6565–6576, doi:10.5194/acp-8-6565-2008, 2008.

ACPD
10, 24135–24169, 2010

Wendisch, M., Pilewskie, P., Pommier, J., Howard, S., Yang, P., Heymsfield, A. J., Schmitt, C. G., Baumgardner, D., and Mayer, B.: Impact of cirrus crystal shape on solar spectral irradiance: a case study for subtropical cirrus, J. Geophys. Res., 110, D03202, doi:10.1029/2004JD005294, 2005.

ACPD
10, 24135–24169, 2010

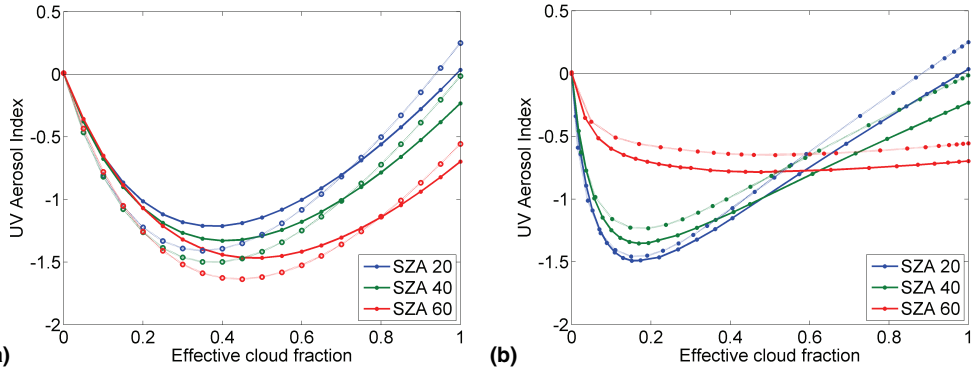

Fig. 1. Results from RTM calculations using SCIATRAN3.0. Henyey-Greenstein cloud parameters are given in the text, but asymmetry parameter was set to 0.87 (dots, solid line) or 0.75 (circles, dotted line). Viewing geometry is nadir, and three solar zenith angles were modelled, as indicated in the figure legend. **(a)** Thick clouds; **(b)** thin clouds (see the text for details).

ACPD
10, 24135–24169, 2010

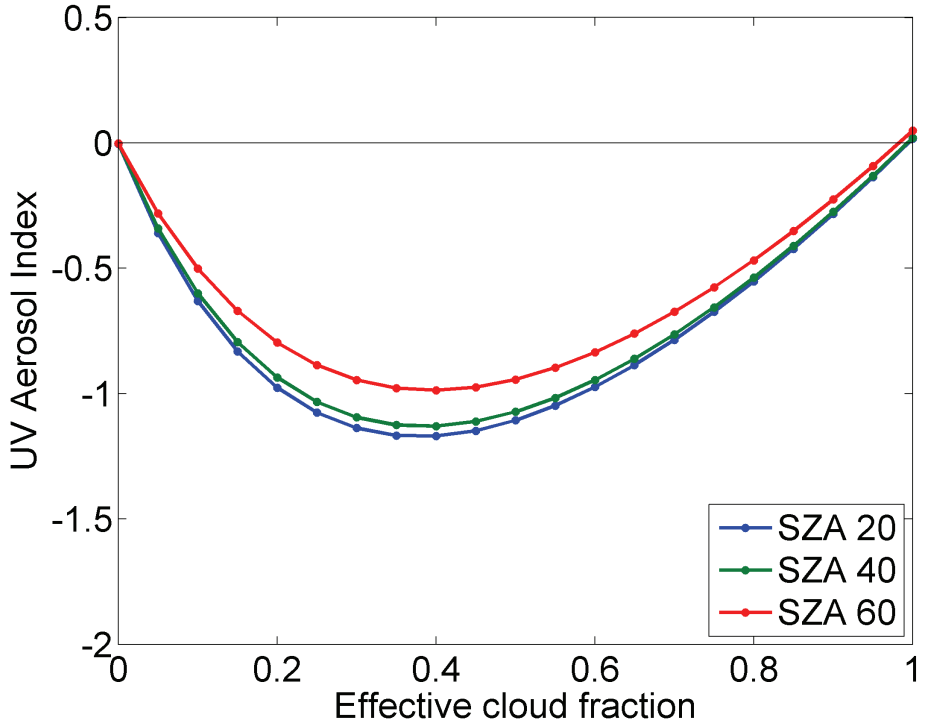

Fig. 2. Results from RTM calculations using SCIATRAN3.0. The clouds are modelled as a Lambertian reflector with albedo = 0.80, located at an altitude of 1 km. Viewing geometry is nadir, and three solar zenith angles were modelled, as indicated in the figure legend. Albedo of the underlying surface was set to 0.05.

ACPD
10, 24135–24169, 2010

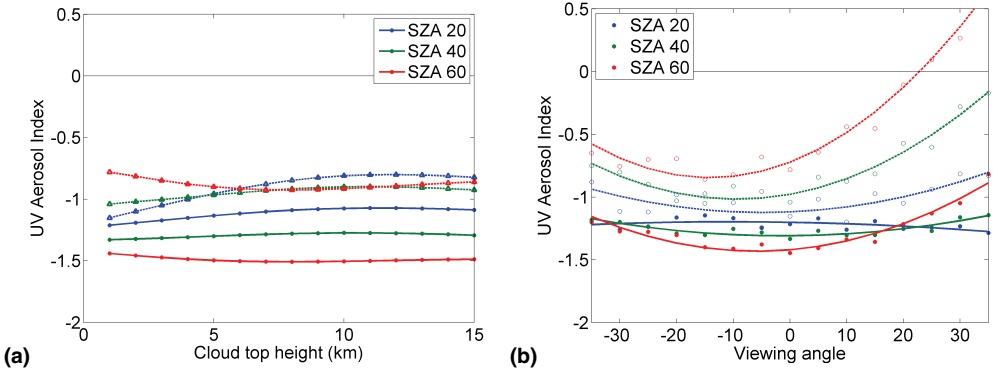

Fig. 3. Results from RTM calculations using SCIATRAN3.0. Cloud parameters are given in the text. Thick clouds (solid lines and dots) have a geometrical cloud fraction of 0.4; thin clouds (dashed lines and triangles) have an optical thickness of 10. All clouds have a geometrical thickness of 1 km. Viewing geometry is nadir, and three solar zenith angles were modelled, as indicated in the figure legend. **(a)** Clouds with nadir viewing geometry and varying cloud top height. **(b)** Clouds with cloud top height equal to 1 km and varying viewing angles. Positive viewing angles denote viewing direction towards the sun.

ACPD
10, 24135–24169, 2010

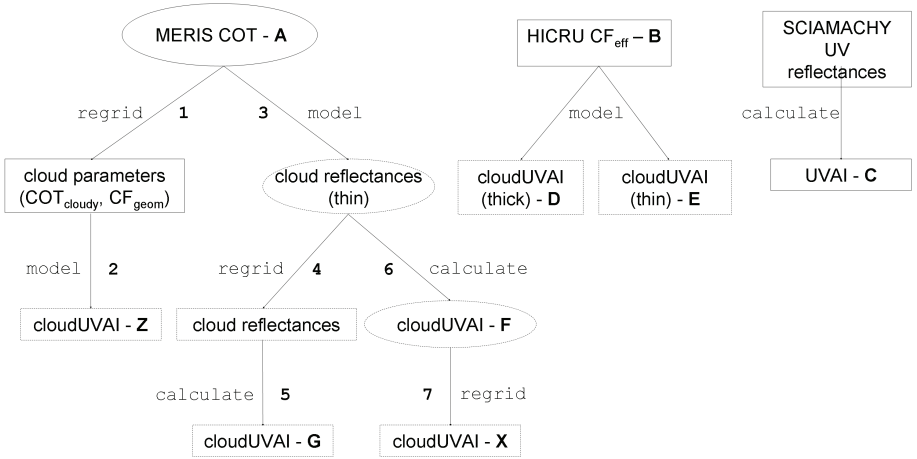

Fig. 4. Flow chart of the calculation of cloudUVAI from MERIS and SCIAMACHY cloud parameters. Rectangles symbolize quantities with SCIAMACHY spatial resolution ($30\times60\,km^2$), whereas ovals indicate MERIS spatial resolution ($1\times1\,km^2$). Boxes with solid borders represent measured values; dashed borders show quantities which were derived from modelled clouds. Capital letters A to G (in bold font) refer to the data in corresponding panels in Figs. 5 and 6; the cloudUVAI data from the boxes marked "X" and "Z" are mentioned in the text in Sects. 3–5, but are not presented in this paper. The individual steps (labelled with "calculate", "model" and "regrid") are explained in the text.

ACPD
10, 24135–24169, 2010

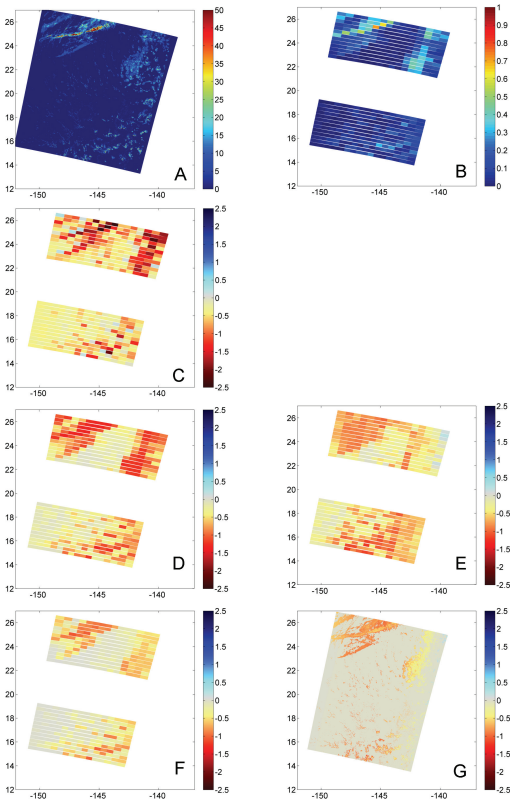

Fig. 5. Case study of cloudUVAI for SCIAMACHY states 8 and 9 in orbit 191033 (16 January 2005). Panel **(A)**, MERIS cloud optical thickness; **(B)**, HICRU effective cloud fraction; **(C)**, SCIAMACHY UV Aerosol Index; **(D)**, calculated cloudUVAI calculated from HICRU CF_{eff} (for thick clouds); **(E)**, cloudUVAI calculated from HICRU CF_{eff} (for thin clouds); **(F)**, cloudUVAI calculated from MERIS COT (for thin clouds) at SCIAMACHY resolution; **(G, F)**, cloudUVAI calculated from MERIS COT (for thin clouds) at MERIS resolution (for details, see text).

ACPD
10, 24135–24169, 2010

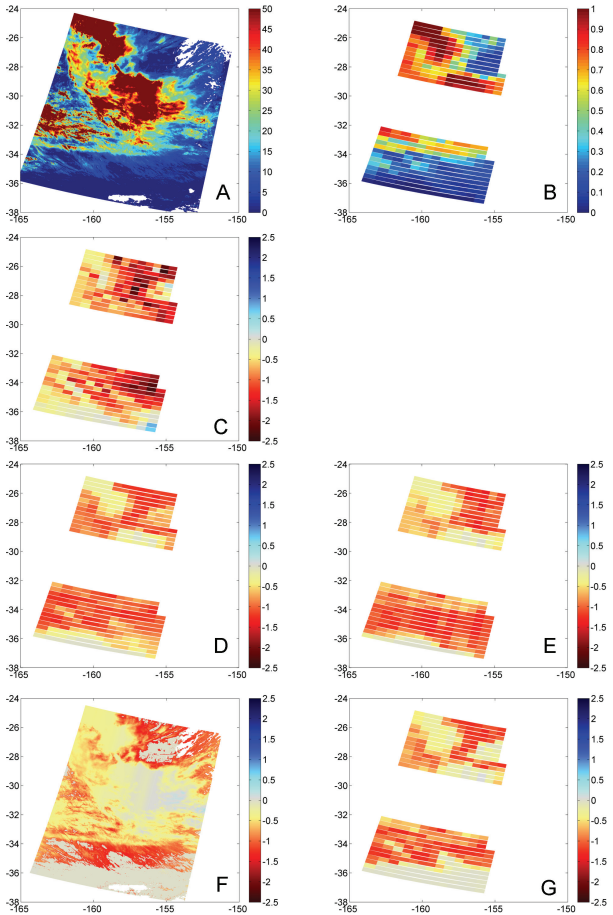

Fig. 6. Case study of cloudUVAI for SCIAMACHY states 15 and 16 in orbit 191033 (16 January 2005). See the caption of Fig. 5 and the text for details.

ACPD
10, 24135–24169, 2010

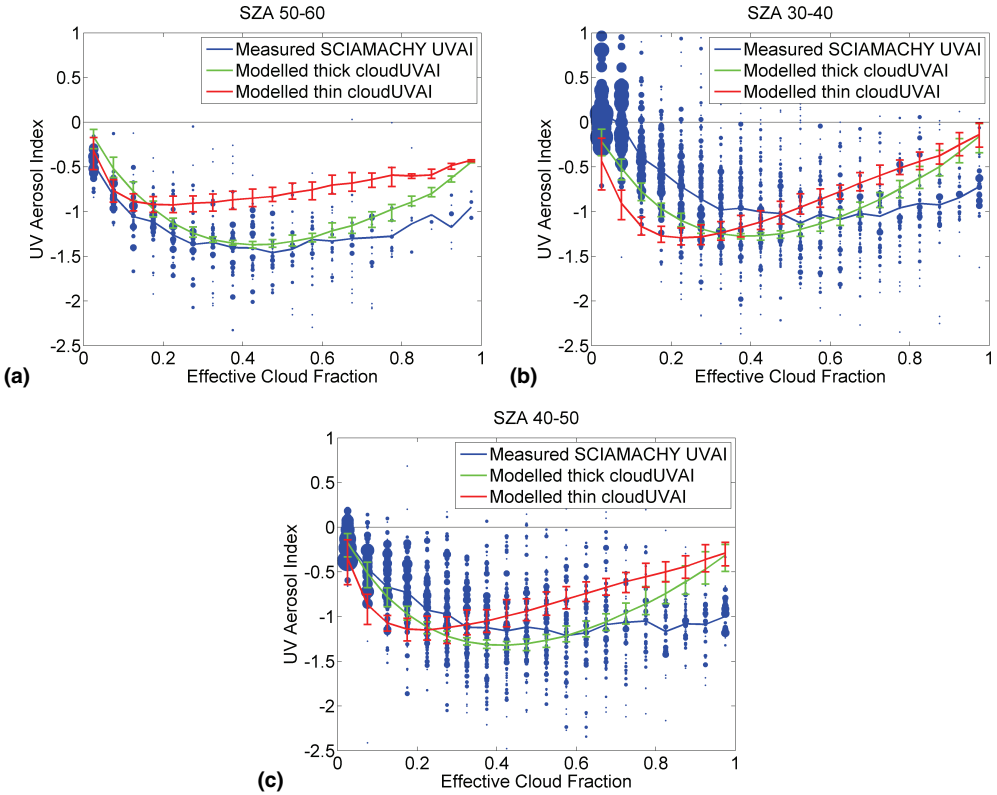

Fig. 7. Seasonally-averaged measured (blue) and calculated (green and red) UVAI values for a region over the South-Eastern Pacific Ocean (20–40° S, 100–180° W). Dots indicate daily mean values, with the size of the point representing the number of data points included in the mean; lines connect monthly mean values. Error bars on the cloudUVAI means represent the spread of the values (i.e., the maximum and minimum daily averaged cloudUVAI). **(a)** SZA between 30° and 40°; **(b)** SZA between 40° and 50°; **(c)** SZA between 50° and 60°. The viewing geometry is near-nadir, with LZA between −10° and +10°.

ACPD
10, 24135–24169, 2010

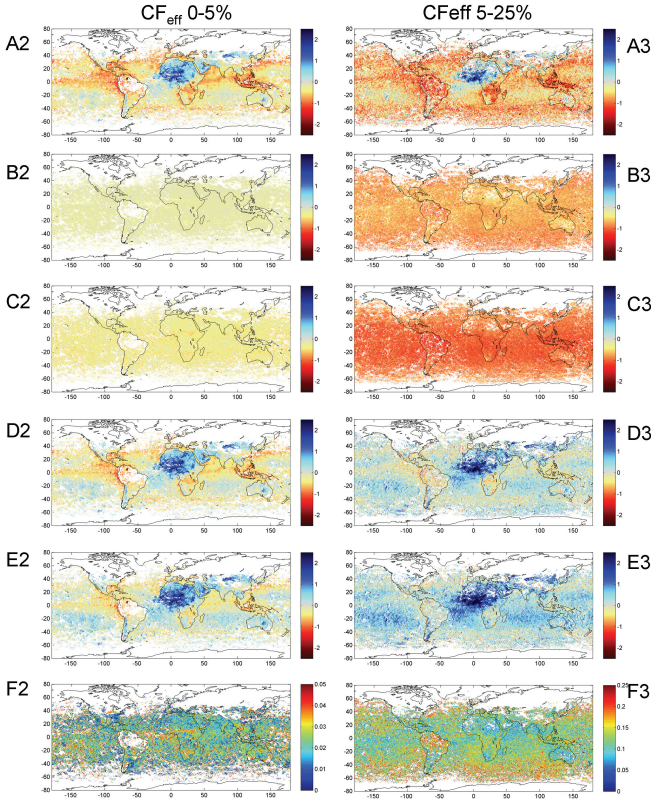

Fig. 8. Seasonally averaged measured and calculated UVAI and cloud fraction for January–March 2005. The data were filtered by effective cloud fraction: left column, CF_{eff}<5%; right column, 5%<CF_{eff}<25%. The panels show, from top to bottom: **(A)** SCIAMACHY UVAI data, **(B)** modelled cloudUVAI (for thick clouds), **(C)** modelled cloudUVAI (for thin clouds), **(D)** difference between UVAI and cloudUVAI (thick clouds), **(E)** difference between UVAI and cloudUVAI (thin clouds), **(F)** HICRU effective cloud fraction (with varying colour bar). See the text for details.

ACPD
10, 24135–24169, 2010

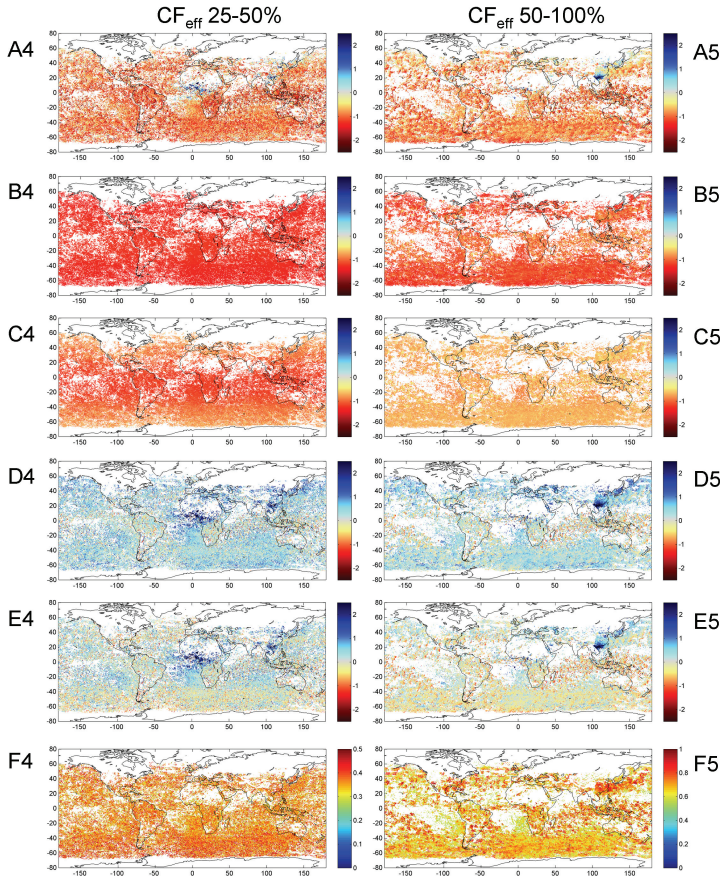

Fig. 9. Seasonally averaged measured and calculated UVAI and cloud parameters for January–March 2005. See the caption of Fig. 8 and the text for details. The data were filtered by effective cloud fraction: left column, 25%<CF_{eff}<50%; right column, 50%<CF_{eff}<100%.

ACPD
10, 24135–24169, 2010

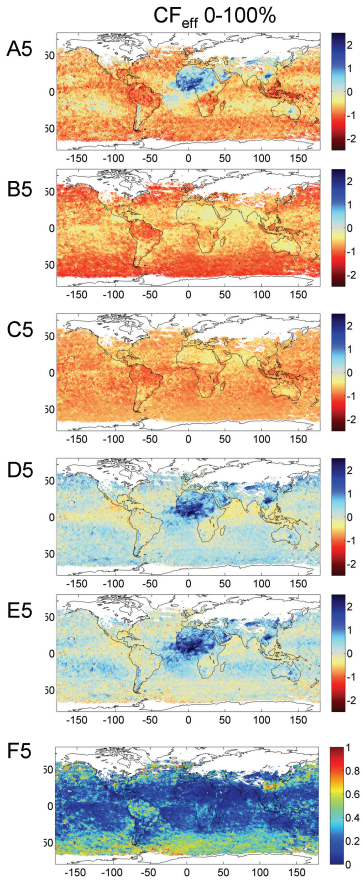

Fig. 10. Seasonally averaged measured and calculated UVAI and cloud parameters for January–March 2005. See the caption of Fig. 8 and the text for details. No cloud filter was applied to the data.

ACPD
10, 24135–24169, 2010